Modeling of multi-fractional suspended particle pathways in a shallow water basin under influence of strong winds

Elena Alekseenko, A.A. Sukhinov, B. Roux

▶ **To cite this version:**

Elena Alekseenko, A.A. Sukhinov, B. Roux. Modeling of multi-fractional suspended particle pathways in a shallow water basin under influence of strong winds. Regional Studies in Marine Science, 2024, 73, pp.103477. 10.1016/j.rsma.2024.103477 . hal-04515082

HAL Id: hal-04515082
https://hal.science/hal-04515082

Submitted on 21 Mar 2024

HAL is a multi-disciplinary open access archive for the deposit and dissemination of scientific research documents, whether they are published or not. The documents may come from teaching and research institutions in France or abroad, or from public or private research centers.

L'archive ouverte pluridisciplinaire **HAL**, est destinée au dépôt et à la diffusion de documents scientifiques de niveau recherche, publiés ou non, émanant des établissements d'enseignement et de recherche français ou étrangers, des laboratoires publics ou privés.

Modelling of multi-fractional suspended particle pathways in a shallow water basin under influence of strong winds

E. Alekseenko[a,b,*], A.A. Sukhinov[c], B. Roux[d]

[a] *Université du Littoral Côte d'Opale, 1, place de l'Yser, BP 1022, 59375, Dunkerque, France*
[b] *Laboratoire d'Océanologie et de Géosciences, CNRS, LOG UMR 8187, 28 avenue Foch, BP 80 62930 Wimereux, France*
[c] *Don State University, Rostov-on-Don, Russia*
[d] *Aix-Marseille Université, CNRS, Centrale Marseille, M2P2 UMR 7340, 13451 Marseille, France; bernard.roux@univ-amu.fr*

Abstract

In this study, we investigate the complex dynamics of multi-fractional suspended particle transport in a shallow water basin subjected to strong wind conditions. Our research focuses on understanding the interplay between wind-induced advection and particle settlement, and its implications for sediment redistribution.

Through our analysis, we reveal the distinct behaviors of different sediment fractions. Clay particles, constituting the lowest fraction in sediment cores, remain suspended throughout the simulation due to their low settlement velocity, with relatively stable concentrations. Conversely, the dominant fraction, medium silt, is suspended during intense wind events but quickly settles to the bed due to its higher settling velocity. Wind stress exceeding 0.05 Pa triggers particulate matter erosion, leading to its presence in the water column.

Additionally, we explore the 2D distribution of sediment characteristics, including thickness, dry density, and mud fraction, to identify areas prone to erosion and deposition. Our findings demonstrate that coastal areas of the Taganrog Bay experienced significant erosion following strong wind events,

*Corresponding author
Email address: elena.alekseenko@univ-littoral.fr (E. Alekseenko)

exhibiting the thinnest sediment thickness and the highest dry bulk density. Deposition areas, characterized by thicker sediment layers and lower dry density, were often found in proximity to erosion zones, indicating the influence of particle resuspension and settlement processes.

Furthermore, we analyze the implications of our findings on the vulnerability of specific regions to erosion and deposition. The central part of the sea contains moderately thicker sediment layers with a moderately high mud fraction, representing a zone of fine sediment accumulation. These fine sediments, including fine silt and clay, remain suspended for longer durations and are redistributed over greater distances by currents.

Overall, our study provides valuable understanding into the multi-fractional suspended particle pathways and their interaction with strong winds in shallow water basins. The results contribute to a better understanding of sediment dynamics, which has implications for coastal management, environmental monitoring, and the preservation of benthic ecosystems.

Keywords: suspended sediment transport, sediment dynamics, wind-induced advection, particle settlement, shallow water basins, sediment fractionation

---

1. Introduction

Coastal areas play a pivotal role in both ecological and socioeconomic context, boasting rich biodiversity and elevated population density along their shores (Arkema et al., 2013; Barbier et al., 2011; Duarte et al., 2013; Martinez et al., 2007; Yang et al., 2020). Despite their significance, these regions are susceptible to various stressors, with the increasing frequency of extreme events along coastlines being a significant consequence of global climate change (IPCC, 2022). Semi-enclosed seas, like the Azov Sea, stand out due to their limited area and depth, making them particularly vulnerable.

The Azov Sea region in the early 21st century witnessed impactful weather-related disasters (Berdnikov et al., 2018), including a severe storm in the Kerch Strait (2007), extreme sea surges in the Don River delta (2013, 2014). The Azov Sea coast faces intensive degradation, with over 50% of the Taganrog Bay coastal zone at a high risk of landslides (Ivlieva and Berdnikov, 2005). The consequences of these storms are often catastrophic, resulting in coastal destruction and extensive erosion (Berdnikov et al., 2018; Yaitskaya,

2022). These effects pose significant challenges to the coastal communities and ecosystems in the region.

As a significant driver of ocean energy, winds, especially during storms, play pivotal roles in reshaping coastal sediment distribution and morphological evolution (e.g., Yang et al., 2023; Colosimo et al., 2023). However, owing to the variability in physical conditions (hydrodynamics, geomorphology, etc.), the impact of winds on sediment transport varies significantly from one coastline to another. Consequently, there is an urgent need for regional case studies on the effects of wind, particularly during storm events, on coastal processes. These detailed investigations are essential for developing a nuanced understanding of the intricate interplay between wind dynamics and coastal morphology in the Azov Sea region.

The processes of erosion and the transport of particulate matter in shallow water basins are often influenced by a combination of climatic and anthropogenic factors and their complex interactions. In the case of the Azov Sea, the interaction between wind, currents, bottom friction (which is influenced by the shallow depth and coastline), erosion processes, and the transport of particulate matter remains poorly understood. Key questions regarding areas vulnerable to erosion and areas where eroded sediments tend to accumulate have yet to be answered.

In addition to the quantity of sediment, the quality of the sediment has significant implications for downstream areas of the Azov Sea. Eroded sediments may contain contaminants such as heavy metals, nutrients, pesticides, and other organic micro-pollutants, posing a threat to the ecological health of the sea. Despite a decline in industrial activities since the 1990s, the ecological state of the Azov Sea remains under strain (Chichaeva et al., 2020). The presence of major industrial centers along the coastline contributes to its classification as one of the highly polluted seas (Klenkin & Agapov, 2011).

Accurate predictions of suspended matter distribution and the subsequent alterations in sediment following storm events in vast shallow water bodies, exemplified by the Azov Sea, are crucial. To meet this imperative, a complex three-dimensional model must be coupled, seamlessly integrating hydrodynamic and sediment transport processes unique to the Azov Sea. This modeling approach provides a nuanced understanding of diverse phenomena shaped by weather and climatic conditions. This includes the emergence of hypoxia zones, a consequence of the accumulation and decomposition of suspended particles in the water column. Moreover, it grants a comprehensive understanding of dynamic changes in bottom topography, shifts in current

patterns, and the silting of shipping channels, directly jeopardizing navigation safety.

In this research, we develop a coupled modeling approach to examine the complex dynamics of multi-fractional suspended particle transport in a shallow water basin subjected to intense wind conditions. Sections 2 and 3 delve into the study site features and the developed coupled model for the Azov Sea, emphasizing the interplay between hydrodynamics and sediment transport. Section 4 concentrates on comparing the model with satellite data. Section 5 reveals results emphasizing the influence of river outflow and wind stress on suspended particulate matter (SPM) stocks and fluxes, while also scrutinizing the 2D distribution of suspended sediment and bottom sediment characteristics, pinpointing areas prone to erosion and deposition. Section 6 draws conclusions from our findings and discusses their implications for the vulnerability of specific regions.

2. Study site

This study has been conducted for the specific case of the semi-enclosed water basin known as the Azov Sea, which is renowned as the world's shallowest sea (Fig. 1). Located in Eastern Europe between 34^oE,45^oN and 40^oE,48^oN, it is connected to the Black Sea through the 4 km long Kerch Strait. The average water depth in the sea is 7 m, with a maximum depth of 14 m. The Azov Sea spans an area of 360 km in length and is 180 km wide.

Due to the narrow inflow of water from the Azov Sea into the Black Sea, it retains a consistently low salinity level. The physical volume, chemical composition, biomass, and fish stocks of the Azov Sea (Fig. 1) are dependent on the volume and quality of freshwater inflow from continental runoff. Each year, approximately 12% of the sea's total volume (320 km^3, equivalent to 39.6 km^3) is replenished in this manner. However, the construction of reservoir dams, particularly on major rivers such as the Don and Kuban, has resulted in a decrease in the overall volume of water flowing into the sea, leading to changes in its composition. Such significant changes in the terrigenous matter supplied to the Azov Sea have occurred in recent decades (Sorokina and Berdnikov, 2008). Apart from dam constructions, other factors contributing to these changes include climatic influences and anthropogenic impacts on the solid runoff formation in river watersheds.

The interaction of these primary factors significantly influences the distribution of suspended solids in the water column and their settlement at

the seafloor, yet it remains poorly understood. Understanding the contribution of each factor, identifying areas prone to erosion or deposition, tracing the trajectory of suspended solids, and determining their final destination (settling areas) are key questions addressed in this study. A 3D modeling of coupled hydrodynamic and sediment transport processes under realistic weather conditions represents the most suitable approach to answer these questions.

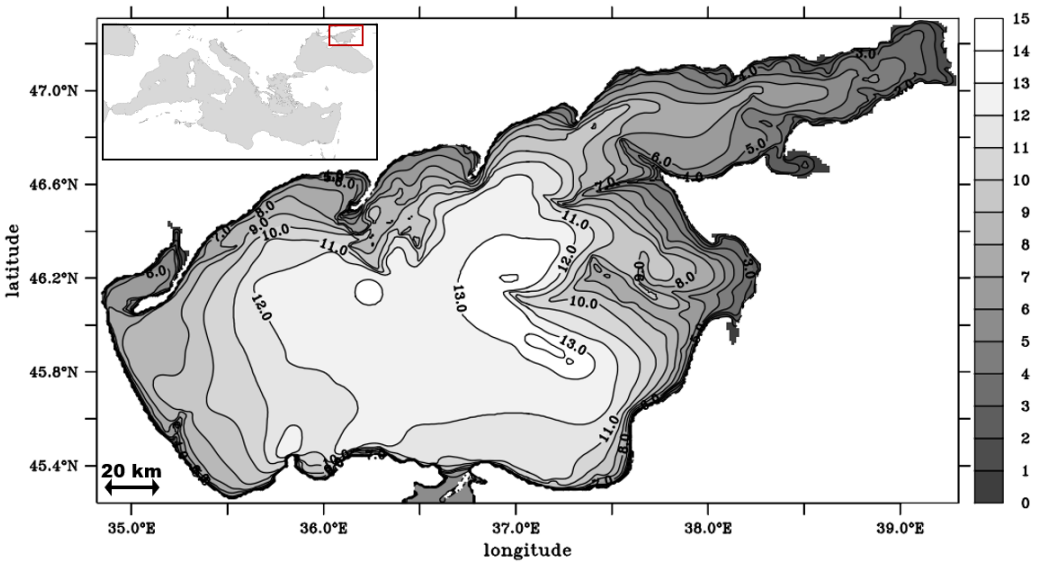

Figure 1: Bathymetric map (in meters) of the Azov Sea. In the small box in the upper-left corner, the sea's geographic position is indicated, along with its connection to the Black and Mediterranean Seas.

The present study focuses on a specific period in June 2021, which experienced a series of extreme events, including strong storms on June 16 and 17. The press service of the Main Directorate of the Emergency Ministry reported various episodes of squally winds reaching speeds of up to 25 meters per second in the eastern part of the Azov Sea, particularly along the coast of the Yeisk and Temryuk regions. During this time, wave heights ranged from 0.8 to 1.3 meters. These extreme events are expected to have significant implications for sediment erosion and redeposition processes.

It is important to consider the continuous influx of terrigenous suspended solids from the Don River, in addition to the effects of these extreme weather conditions.

3. Model description

Herein, a sediment transport model is coupled with the hydrodynamical model. The main equations and features of the sediment transport model have been detailed by Le Hir et al. (2011), Mengual et al. (2017), and Diaz et al. (2020).

3.1. Hydrodynamics

We use the 3D model of hydrodynamics MARS3D (Model for Applications at Regional Scales) developed by the French Research Institute IFREMER (Lazure and Dumas, 2008; Lazure et al., 2009). Detailed information about MARS3D model : governing equations, boundary conditions, and model discretisation can be seen in Alekseenko and Roux (2020). MARS3D is based on the incompressible Reynolds Averaged Navier-Stokes (RANS) equations in the classical Boussinesq approximation with the hydrostatic assumption. To better take into account the two boundary layers (at the surface, and at the bottom) a refinement of the vertically normalised σ grid is used. MARS3D considers free surface and bottom boundary conditions (see Eqs.2-3 in Alekseenko and Roux, 2020). The bottom boundary condition depends on the bottom roughness z_0 which correspond to the Azov Sea the sediment core samples. The model's spatial resolution is set at 1 km, resulting in a grid of 354 nodes in the X direction and 231 nodes in the Y direction. Additionally, the model incorporates 24 σ layers, refined near the bottom and surface. To ensure numerical stability and meet CFL convergence conditions, a physics timestep of 10 seconds is employed. The coupling with sedimentary transport model computations is invoked every 30 seconds.

The initial conditions for salinity and temperature in the Azov Sea were set at 12 PSU and 20^oC, respectively, resulting in an initial water density of 1007.352 kg/m^3 observed in June.

At the confluence of the Azov Sea with the Black Sea (located at the southern boundary, specifically the Kerch Strait), an open boundary condition was considered with free exchange. Tidal oscillations were neglected due to their low amplitude, ranging from 1 to 3 cm. The salinity level at the Black Sea was assumed to be constant at 18 PSU.

Regarding freshwater inputs, the model took into account the contributions from six branches of the Don River, each with an equal runoff rate (total runoff of 900 m^3/s). Additionally, the Kuban River with non-stationary

climatological runoffs was considered, and corresponding climatic freshwater temperatures were incorporated into the model. The temperature data for the Don River were obtained from world-weather.ru monthly climatology, while the temperature data for the Kuban River were obtained from travel.org.ua monthly climatology.

A simulation period of one month, from June 1, 2021, to July 1, 2021, was selected for this study. The chosen period encompassed three extreme events, as shown in Fig. 4a. One of the events was identified by EMERCOM, with wind gusts up to 25 m/s. Weather conditions for the simulation were obtained from the Modern-Era Retrospective analysis for Research and Applications, Version 2 (MERRA-2) dataset, which covers the Azov Sea for the period from June 1, 2021, to July 1, 2021. The MERRA-2 data was downloaded from https://giovanni.gsfc.nasa.gov and included variables such as 2-m air temperature, atmospheric pressure, relative humidity, 10-m U and V components of the wind (Fig.2 show Azov Sea area averaged values of wind speed and direction), downward solar radiation flux, and infra-red flux.

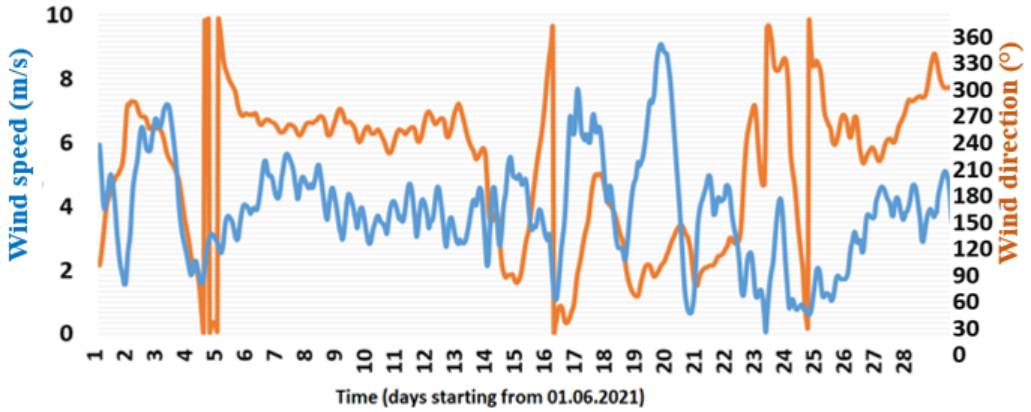

Figure 2: Time evolution of the area-averaged wind speed and wind direction throughout June 2021.

Furthermore, in order to generate realistic 3D initial fields of salinity, temperature, and current distributions for the subsequent simulation of June 2021, a one-year simulation was conducted using climatological meteorological conditions. This process, known as spin-up, aimed to establish a suitable starting point for the June 2021 simulation and ensure more accurate and reliable results.

3.2. Sediment transport

Concerning the sediment transport, we use the sediment module MUSTANG (MUd and Sand TrAnsport modelliNG, Diaz et al. 2020) coupled with MARS3D model and also provided by IFREMER (Le Hir et al, 2011; Cayocca et al, 2014). MARS3D model manages particle advection in the water column, according to a 3D framework, whereas MUSTANG module manages particle settlement in the water column as well as exchanges with the bed by erosion, deposition, and consolidation processes in the bed. In MUSTANG module, processes such as deposition and erosion are modelled for each horizontal cell (dx*dy) separately (1D model, see Fig.5 in Cayocca et al, 2014), with a variable number of layers whose thickness, porosity and concentration vary with time by sedimentation and resuspension events.

The modelling techniques in sediment transport simulations are split into two classes (Le Hir et al., 2011):

- "for non cohesive sediment (sand and gravel), sediment evolution is computed by solving a continuity equation (Exner equation) where erosion or deposition result from the divergence of a transport capacity related to the hydrodynamic regime; this method is suitable when equilibrium is reached rapidly, which is the case for sediment with high settling velocity;

- for fine sand and mud that are mostly transported in suspension, an advection/diffusion equation is solved (either depth-integrated or not) and the sediment evolution is straightforwardly deduced from erosion and deposition rates".

Le Hir et al. (2011) described in detail the sediment transport modelling strategy which offers the possibility to account: "simultaneous bed load and suspended sediment transport, mixing of several sediment classes in the water column as well as in the sediment, consolidation of muddy and mixed sediments with possible segregation of sand particles by adapting Gibson theory, management of erosion fluxes depending on the cohesive or non-cohesive nature of the superficial sediment. Special attention was paid to the way the sediment layers content is updated after deposition, in order to simulate possible pore filling up between large particles in superficial sediment before creating a new layer".

Le Hir et al. (2011) described the computation of suspended transport by solving an advection-diffusion equation (Eq. 2) for the concentration of

different particle classes. These classes are categorized into three types based on their behavior, as defined by the authors:

- Coarse type: This type represents non-cohesive particles that are exclusively transported as bedload. It is typically assigned to coarse sand but can also be extended to include gravels, cobbles, and pebbles.

- Sand type: This type represents non-cohesive particles that are transported in suspension. It refers primarily to fine sand but can also include medium sand, as demonstrated by the ability to simulate transport capacities through an advection-diffusion process (Waeles et al., 2007).

- Mud type: This type represents cohesive particles that are naturally transported in suspension. These particles are likely to flocculate, leading to variations in settling velocity, and can undergo consolidation within the bed. The mud type is commonly associated with silt and clay particles but can also be used to represent organic matter.

By classifying particles into these three types, the model can accurately simulate the transport and behavior of different sediment classes, considering their cohesive or non-cohesive nature and their transport mechanisms.

$$\frac{\partial C}{\partial t} = -\frac{\partial Cu}{\partial x} - \frac{\partial Cv}{\partial y} + \frac{\partial CW_s}{\partial z} + \frac{\partial}{\partial z}\left(K_z \frac{\partial C}{\partial z}\right) + E - D \tag{1}$$

Where C - sediment concentration in water, W_s - particle settling velocity, K_z - coefficient of vertical turbulent exchange, E - erosion flux and D - deposition flux, (u, v) - velocity components along coordinates (x, y).

MUSTANG model incorporates a pore filling procedure, as described by Le Hir et al. (2011) and illustrated in Fig. 5a and 5b of their study. This procedure involves the sequential filling of sedimentary layers with coarser particles, such as gravels and sands, followed by the filling of the pore spaces between these particles with mud-type particles until the critical concentration of the mixed sediment is achieved. This pore filling procedure is employed to obtain a mixed mud-sand sediment in the initial sediment column and is applied at each time step during the sedimentary dynamics calculation in MARS3D.

In MUSTANG model, the maximum volumetric concentration (which represents the volume of a specific particle type divided by the total volume of

the fluid-particle mixture) for sorted sand and mud-sand sediment, typical for the studied area, must be respected. This requirement applies to any combination of particle types, as shown in Fig. 1 of Le Hir et al. (2011).

For the representation of sediment in the Azov Sea in this study, a total of 10 sediment sublayers are considered.

3.3. Sediment granulometry data and main size classes

Implementing a sediment transport model poses a significant challenge in selecting the particles as state variables, as natural size spectra are continuous, and the computational cost rises with an increasing number of state variables. In this study, the sediment characteristics were derived from Arkhipov et al. (2010), which provides information on the sizes and fractions of suspended sediment particle classes in the Azov Sea (as shown below).

Firstly, the median diameter $d_{50} = 20$ μm of all presented size classes corresponds to the medium silt. After Nikuradze formulation: $z_0 = 3d_{50}/30$, such a d_{50} corresponds to $z_0 = 2$ μm.

Furthermore, we divide the average sediment granulometry into six particle size ranges and determine the representative particle size and its corresponding fraction for each size class in order to facilitate sediment transport modeling.

6 particle sizes have been selected for our model (Arkhipov et al., 2010) corresponding to 2 particle sizes of sand type, 3 particle sizes of mud type, and 1 particle size of clay type; i.e. : 14% of fine sand of 150μm, 18% of very fine sand of 80μm, 18% of coarse silt of 60μm, 46% of medium silt of 30μm, 2.8% of fine silt of 7.5μm, and 1.2% of clay of 1μm .

In addition to selecting sediment particles and their fractions, our model requires two values for the maximum volumetric concentration: one for pure sand and another for the mixed sediment found in the Rove channel. For pure sand, we use a maximum value of 0.58, as suggested by Soulsby (1997) and also employed by Le Hir et al. (2011) and Mengual et al. (2017). As for the mixed sediment, we follow the soil classification triangle recommended by the USDA (US Department of Agriculture), which is based on separate sand, silt, and clay fractions (USDA, 2014). According to this classification, the mixed sediments in the Azov Sea correspond to the "silt loam" type, with a maximum volumetric concentration of 0.5.

Regarding sediment density, we adopt the option provided by MUSTANG package, where a density of 2650 kg/m^3 (corresponding to quartz) is used for all grain sizes.

sed. size (μm)	150	80	60	30	7.5	1
BSS^D_{cr} (N/m^2)	0.155	0.120	0.1	0.08	0.035	0.005
W_s (m/s)	Souslby	Soulsby	1.11e-3	5.4e-4	4.2e-5	8.58e-7

Table 1: Modelled bottom shear stresses for deposition and settlement velocities.

3.3.1. Deposition

MUSTANG model incorporates a sedimentation process, the formulation of which is provided by Le Hir et al. (2011). The general formulation for the sediment deposition flux follows Krone's law:

$$D = W_{si} C_i \left(1 - \frac{BSS}{BSS^D_{cr}}\right). \tag{2}$$

As input parameters we need to provide settling velocities W_s of the different suspended sediment particles and their critical shear stresses for deposition BSS^D_{cr}. BSS^D_{cr} we estimated following Berenbrock&Tranmer (2008) formulation. For the four cohesive substances (silts and clay), the settling velocity is considered to be constant (i.e. we do not take into account a flocculation process) and has been estimated using the Stokes law (the maximal limit of settlement velocity). For non-cohesive particles (sands), the settling velocity is taken from Soulsby formulation (after Le Hir et al.,2011, Dufois & Le Hir, 2015). Table 2 resumes input parameters needed to MUSTANG to simulate deposition process.

For the deposition process, in the case if all sediment sublayers are filled up, MUSTANG model provides additional upper sublayers to be filled by settled particles.

3.3.2. Erosion

In MUSTANG model the erosion flux is based on the formulation from Partheniades (1965) with erosion rate E expressed as a function of the excess-shear stress to a power:

$$E = E_0 \left(\frac{BSS}{BSS^E_{cr}} - 1\right)^n, \text{if } BSS > BSS^E_{cr}. \tag{3}$$

MUSTANG erosion parametrization depends on the fraction of the cohesive sediment (mud). Three different regimes of erosion are considered:

(i) the sediment behaves as non-cohesive sediment below a first critical mud fraction ($fm1_{cr}$), so the prescribed erosion regime follows the formulation of pure sand erosion; (ii) above a second critical mud fraction ($fm2_{cr}$, Le Hir et al., 2011), a cohesive erosion behavior is defined; and (iii) for an intermediate content of mud ($fm1_{cr} < fm < fm2_{cr}$) a transitional erosion behaviour of the mud-sand mixture is considered; and in this case an interpolation method of erosion rate is prescribed between non-cohesive and cohesive erosion rates.

Le Hir et al (2011) describes in detail such an erosion regimes, for which erosion rate constant E_0 and power law number n for pure sand and pure mud should be determined in accordance with the nature of modelled sediments. An interpolation method for E_0, BSS^E_{cr} and n among two specified (exponential or linear) should be chosen within MUSTANG.

In the model bottom shear stress formulation for erosion (BSS^E_{cr}) of pure sand is determined following the Shields criteria formulated by Soulsby (1997). For the pure mud, bottom shear stress formulation for erosion (BSS^E_{cr}) is varying with the consolidation state of the sediment and follows a classical power law depending on mud concentration (Le Hir et al., 2011; Waeles et al., 2008).

For the studied case of the Azov Sea, typical values for the limits of pure sand and pure mud erosion behaviours have been chosen ($fm1_{cr}$=0.2 and $fm2_{cr}$=0.7) the same as in Le Hir et al. (2011) and Mengual et al. (2019). Power law number n for the erosion equation Eq.5 in the cases of the pure sand and pure mud have been also chosen the same as in Le Hir et al. (2011) and Mengual et al. (2019) and equal to 1.5 and 1 respectively. Linear interpolation between values of E_0, n and BSS^E_{cr} have been chosen for a transitional erosion behaviour (mixed mud/sand sediment case). Erosion rate E_0 for pure sand was set to an experimental value of $5.94*10^{-3}$ kg/s/m^2 for 200μm grain size (Mengual et al, 2019). For the pure mud, erosion rate E_0 was set to $2*10^{-3}$ kg/s/m^2 - value taken from Torfs (1995) for surface erosion of muddy sediments.

3.3.3. Consolidation

The consolidation model employed in this study follows the modeling approach introduced by Le Hir et al. (2011) and subsequently updated by Grasso et al. (2015). The consolidation model incorporates the Gibson equation to account for segregation processes, permeability, and effective stress regimes during the sedimentation and consolidation phases (Grasso et al., 2015). Grasso et al. (2015) conducted numerical simulations of mud-

sand mixture consolidation based on data obtained from settling column experiments. This version of the consolidation model has demonstrated its ability to accurately simulate sedimentation and consolidation processes for mixed sediments with a moderate to large sand content (15 to 50%). Grasso et al. (2015) provided a set of parameters that yield a reasonable level of predictive accuracy for mixed-sediment consolidation within a 3D sediment transport model.

In this study, we adopt a formulation for simulating the permeability process proposed by Grasso et al. (2015). It involves a combination (using the minimum function) of two different formulations to compute the constitutive relationship for permeability. The first formulation is associated with the void ratio (as described by Bartholomeeusen et al., 2002 and Le Hir et al., 2011), while the second formulation considers the relative volume fraction of fine particles based on the fractal theory introduced by Merckelbach and Kranenburg (2004). Among the numerous experimental data utilized for parameterizing the permeability model presented by Grasso et al. (2015), the experimental sample MSMB-C2 from Cancale Beach in the Bay of Mont Saint-Michel exhibits the closest similarity to the sediment mixture in the Rove channel, as it contains approximately 15% sand content. Therefore, we have selected the set of individual parameters for MSMB-C2 detailed in their Table 3, which demonstrated high prediction skills (with $r^2 = 0.994$ and $e_{rms} = 0.06$) for this work.

3.3.4. River outflows and initial concentrations in water

The average annual sediment load carried by the Don River is approximately 0.5 million tons, with the majority of it (92-95%) occurring during the spring flood.

In the year 2021, a significant portion (40-50%) of the total runoff occurred towards the end of May, June, and the first ten days of July due to rain showers. Consequently, the water turbidity during the flood reached approximately 0.35 g/l in May-June 2021, while during other times of the year, it averaged around 0.05 g/l. Thus, the annual average turbidity was approximately 0.23 g/l. In the case of intense rainfall during June-July 2021, the turbidity of the Don River runoff can be assumed to be around 0.30-0.35 g/l. Therefore, a constant value of 0.35 g/l (consistent with the simulated period) has been considered in the model for the Don River, with the same fraction partition as reported in the sediment cores by Arhipov et al. (2010).

Furthermore, we account for the presence of ambient suspended fine par-

ticles in the water that existed prior to the start of the simulated period. A uniform initial concentration of fine particles (fine silt and clay) was set to 0.25 g/l throughout the water column.

4. Model validation

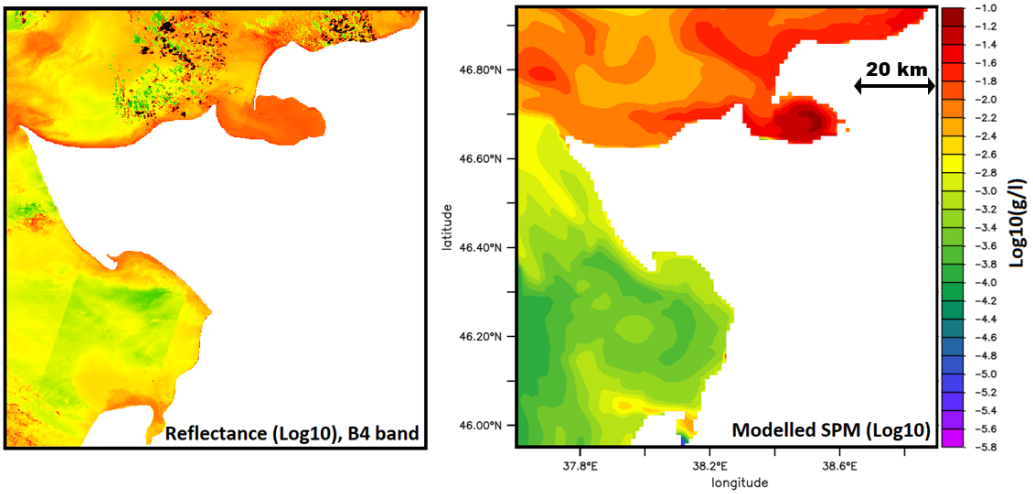

Figure 3: (a) Sentinel2-MSI satellite image of the B4 red color band of 665 nm (representing total SPM at the sea surface of the north-eastern region of the Azov sea, 7 colors palette, LOG10 scale) at 22.06.2021 8h30, (b) modelled SPM concentration at the sea surface at 22.06.2021 at noon.

The coupled model was initiated for a duration of one month, specifically from June 1, 2021, to July 1, 2021. Realistic meteorological conditions were incorporated, taking into account the temporal variation of wind speed, atmospheric pressure, air temperature 2 meters above the sea surface, precipitation, and humidity. These meteorological inputs were obtained from the atmospheric dataset MERRA2. The primary aim of this study was to validate the model outputs concerning SPM concentrations. This validation process aimed to confirm the suitability of the chosen model parameterization for subsequent investigations.

For this study, optical reflectance data (unitless) derived from the Sentinel2 satellite were utilized to analyze SPM. Due to limited availability of data products for the simulated period and the specific study area, the most suitable image with minimal cloud cover was obtained for June 22, 2021, at

8:30 am. This image captured the northeastern region of the Azov Sea, including the shallowest part known as the Taganrog Bay, and was acquired by the Sentinel2-MSI sensor with a spatial resolution of 10m. The data source for this image was peps.cnes.fr. In line with the approaches proposed by Nechad et al. (2016) and Han et al. (2016), the spectral red color band B4 channel with a wavelength of 665 nm was utilized to examine the distribution patterns of SPM on the sea surface. This approach serves as an initial and straightforward method for studying SPM structures.

It is worth noting that prior to the selected date, three wind storm events occurred on June 3, 17, and 20, 2021. These events contributed to sediment resuspension and transport, which should be visible in the satellite image and can be compared with the modeled SPM outputs. Additionally, the satellite image covers two distinct areas within the northeastern part of the sea. The first area is the expansive and shallow Taganrog Bay, located in the southern part, with an average depth ranging from 2 to 4 meters. This area is influenced by inflows from the Don River and experiences significant resuspension processes during strong winds. The second area is the central-eastern deeper region, with depths reaching 8 to 9 meters (Fig.1).

The SNAP tool (step.esa.int) was utilized to analyze the reflectance B4 data, as shown in Fig. 3a. The data was processed using a 7-color palette within the range of 0.03 to 0.2. On the right column of Fig. 3, Fig. 3b illustrates the SPM concentration structure at the sea surface for the same region and date.

From the comparison of Fig. 3a and Fig. 3b, it is evident that the coupled model successfully captures the main characteristics of the satellite-derived structure. The highest concentrations are observed in the Taganrog Bay, particularly along its southern shore, while the lowest concentrations are found in the deeper part of the sea, indicated by a green pattern visible in both figures. This outcome demonstrates that the 3D hydro-sedimentary transport model of the Azov Sea was appropriately parameterized, allowing it to reproduce realistic distributions of SPM. As a result, the model can be utilized for further investigations on sediment resuspension and transport, as presented in this study.

5. Numerical results

5.1. SPM stocks and fluxes are influenced by the outflow of the Don River and wind stress.

This paper examines the impact of two main sources of suspended matter in the Azov Sea: the sedimentary layer, which undergoes resuspension and sedimentation, and the Don River runoff, which carries suspended matter from the land. By modeling hydro-sedimentary transport, we can assess the influence of these processes on the stocks of suspended matter in the water column and sediment, as well as the fluxes of suspended matter between water and sediment.

Figs. 4, 5, and 6 illustrate the evolution of suspended matter stocks and cumulative flows averaged over the selected region's volume. Our focus is on the Taganrog Bay area (shown as a grey subfigure in Fig. 5a) due to its shallow water depth and proximity to the confluence of the Don River. The coordinate range for the Taganrog bay area is 38.75^oN-39.3^oN, 48.75^oE-47.3^oE, with a total volume of approximately 4 km^3.

Fig. 4 illustrates the modeled evolution of stocks for each particle size, utilizing a logarithmic scale to accentuate the variability of the finest particles. Clay particles consistently remain resuspended throughout the simulated period, contributing to a relatively high stock in the water column (approximately 10^8 kg). Notably, the curves for fine silt and clay showcase a smoother profile compared to the curves for coarser grain sizes, attributed to their smaller particle size and settlement velocity, resulting in an extended duration of suspension in water relative to other fractions.

Medium and fine silt stocks exhibit elevated levels for only a few hours between June 2nd and 3rd and June 17th and 21st. Sand stocks display similar curve shapes to silt but with significantly lower concentrations.

Furthermore, it is seen that the peak values of the stock line for fine silt closely resemble those of coarse silt, as opposed to those of medium-sized silt. This correlation is linked to their initial suspended particulate matter (SPM) fraction, which is smaller than the initial fraction of medium silt.

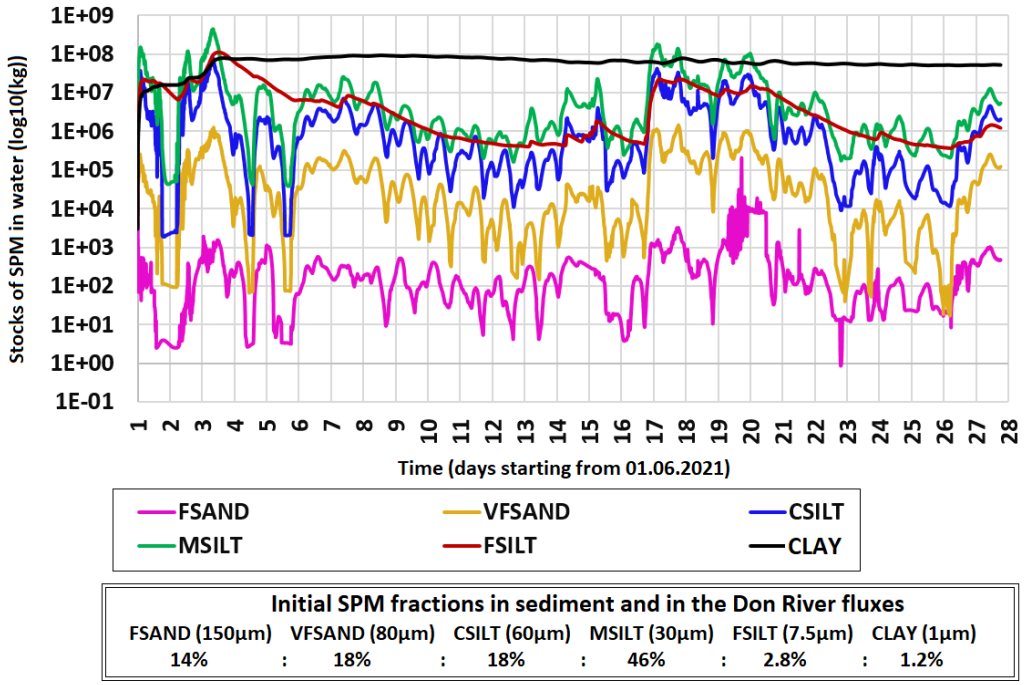

Figure 4: Time-evolution of the stocks in water of SPM (log10(kg)) in the Taganrog Bay area (38.75°N-39.3°N; 48.75°E-47.3°E, volume of approximately 4 km^3).

Fig. 5 provides an information about the wind stress evolution throughout the simulated month (Fig. 5a) and the corresponding evolution of SPM fluxes in the water column associated with resuspension (sediment <-> water fluxes) and influx from the Don River (Fig. 5b). Fig. 5b specifically showcases the evolution of the particles with the highest fractions. On Fig. 5b, a positive slope indicates an increase in flux in the water column or resuspension due to erosion, while a negative slope represents a decrease or deposition. The consistently increasing slopes in the fluxes from the Don River on Fig. 5b demonstrate a constant influx of particulate matter into the Taganrog Bay, as imposed in the model.

By examining Fig. 5a, it is evident that the highest wind stresses exceeding 0.05 Pa on June 2nd-3rd and June 17th-21st align with the patterns observed in the blue curve, primarily corresponding to the resuspension (positive slope) of medium silt particles (MSILT), and to a lesser extent, the resuspension of coarse silt particles (CSILT, magenta curve) shown on Fig. 5b. Medium silt erosion is the most pronounced due to its higher fraction in the sediment (initially 46%). After each event, the slopes decrease, indicat-

ing rapid deposition, primarily attributed to the relatively high settlement speed of these particles (approximately 0.0001739 m/s, equivalent to around 15 m/day). This trend is also observable in the evolution of medium silt stock during and after windy events (Fig. 4).

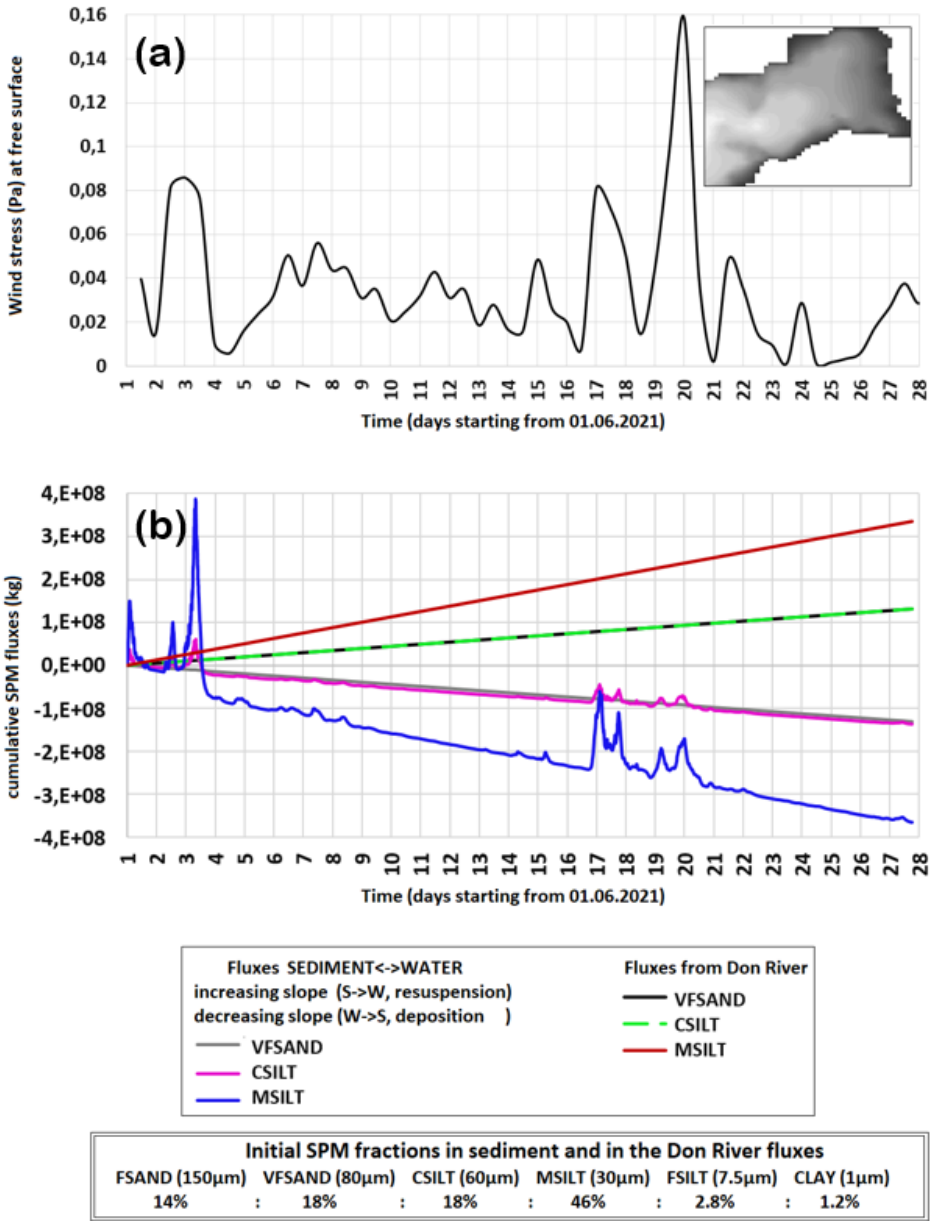

Figure 5: (a) Time-evolution of the wind stress (in Pa) averaged over the Taganrog Bay area (depicted in the top-right corner) corresponding to the wind speed range of 0-9.1 m/s. (b) Time-evolution of the cumulative SPM fluxes (in kg) in the Taganrog Bay area (38.75^oN-39.3^oN; 48.75^oE-47.3^oE, volume of approximately 4 km^3).

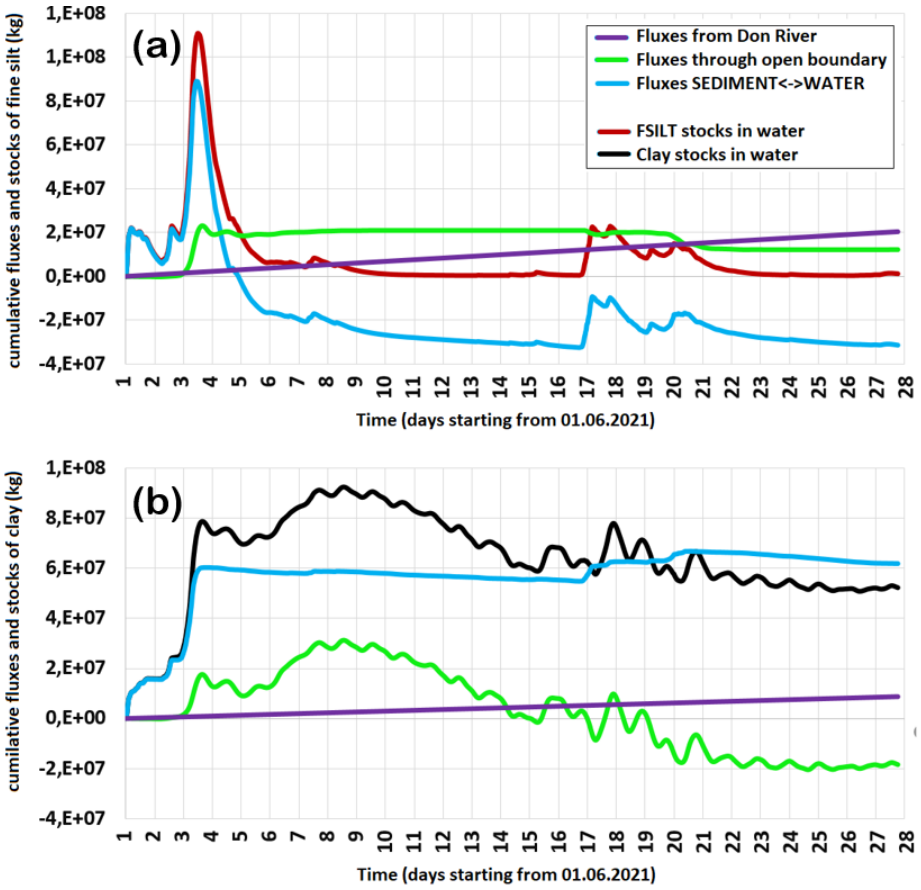

Figure 6: Time-evolution of the stocks and cumulative fluxes (kg) in water of fine silt (a) and clay (b) in the Taganrog Bay area.

Fig. 6 displays fluxes and stocks related to fine particles, specifically fsilt and clay. The Don River flux was set based on its fraction in the sediment (4%), resulting in a very low contribution. During windy events, fine silts undergo resuspension and are subsequently redeposited within 1-2 days, while clay particles remain suspended even after each event. Fluxes at the open boundary of the Taganrog Bay zone indicate that clay particles initially enter the zone during the first 10 days (positive slope), but later, they are transported out of the zone in the subsequent days (negative slope). As for fine silt particles, a couple of days after a wind event, they are redeposited, and the flux through the open boundary remains unchanged. Following the second wind event, some fine silt particles are redeposited, while others exit

the Taganrog Bay area with the currents.

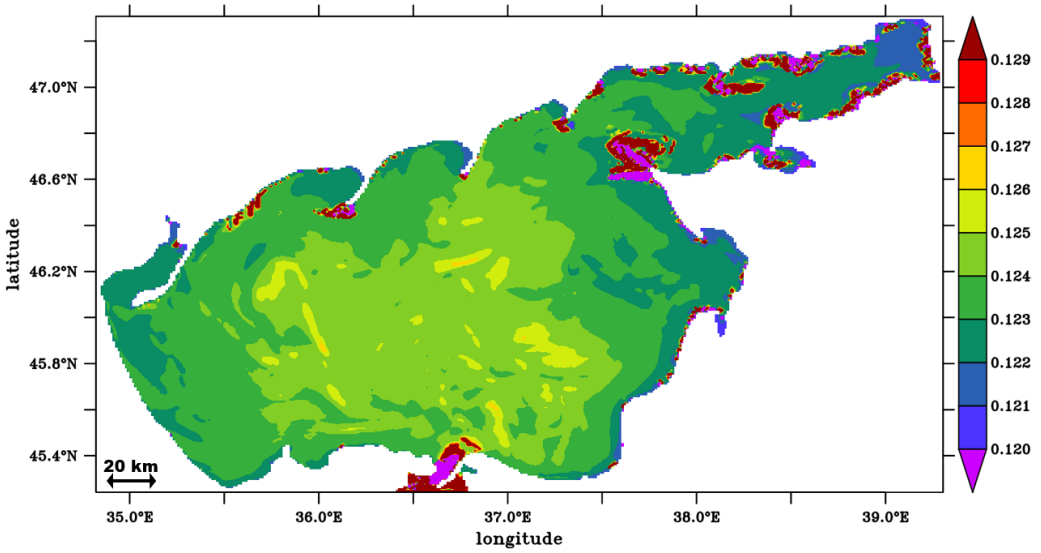

Figure 7: Sediment thickness (m) at July 1st, 2021.

5.2. Areas of erosion and deposition

To gain a better understanding of the sediment's characteristics, such as dry density and fractions, Figs. 7-9 were created to examine the sediment after one month of simulation.

Fig. 7 illustrates the sediment thickness at the end of the one-month period. The thickness demonstrates changes due to consolidation and erosion, as well as deposition. Dark red colors represent areas with the highest sediment thickness, indicating significant deposition. On the other hand, magenta colors highlight areas where the initial sediment layer has undergone extensive erosion. The coasts of the Taganrog Bay experience the highest erosion, leading to the release of suspended solids into the water column, in addition to the contribution from river inflow. Some eroded sediment from the Taganrog Bay coast is redeposited in nearby areas, while finer particles are transported further away (as explained in Figs. 4-6). The remaining colors indicate variations in sediment thickness resulting from a combination of deposition, erosion, and consolidation processes. Without additional information about sediment density and composition, distinguishing areas dominated by deposition and consolidation from those with low erosion and consolidation, particularly in the central part, becomes challenging.

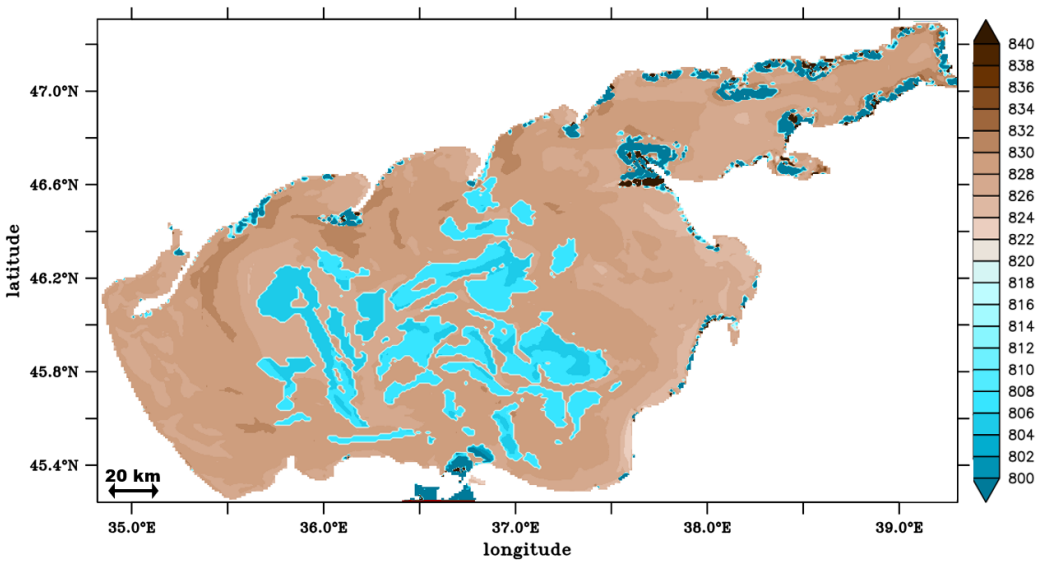

Figure 8: Average dry density of sediment (in kg/m^3) at July 1st, 2021, with an initial mean over sediment thickness dry density set at 347 kg/m^3.

5.3. Properties of the sediment

Fig. 8 presents the dry density of the sediment after one month of simulation. The sediment undergoes three main processes: erosion, deposition, and consolidation. Consolidation is a continuous process influenced by the mud fraction, while erosion and deposition are dependent on the bottom stress, which is comparable to the critical shear stress for the mixed sediment. The final dry density ranges from 800-840 kg/m^3, indicating a significant difference from the initial density of 347 kg/m^3 due to the consolidation process.

Areas represented by light blue colors indicate low density, suggesting minimal changes in sediment over the course of one month, primarily driven by permanent consolidation. Dark blue colors correspond to deposition areas depicted in Fig. 7 (dark red colors), representing regions with the lowest density but higher thickness due to fresh deposition and limited consolidation. Brown colors denote areas in an intermediate state, experiencing a combination of consolidation, erosion, and/or deposition. The darkest brown color indicates erosion-dominated areas, aligning with the regions of the lowest sediment thickness shown in Fig. 7.

Fig. 9 illustrates the distribution of the mud fraction in addition to the sediment dry density. The mud fraction has undergone changes, transition-

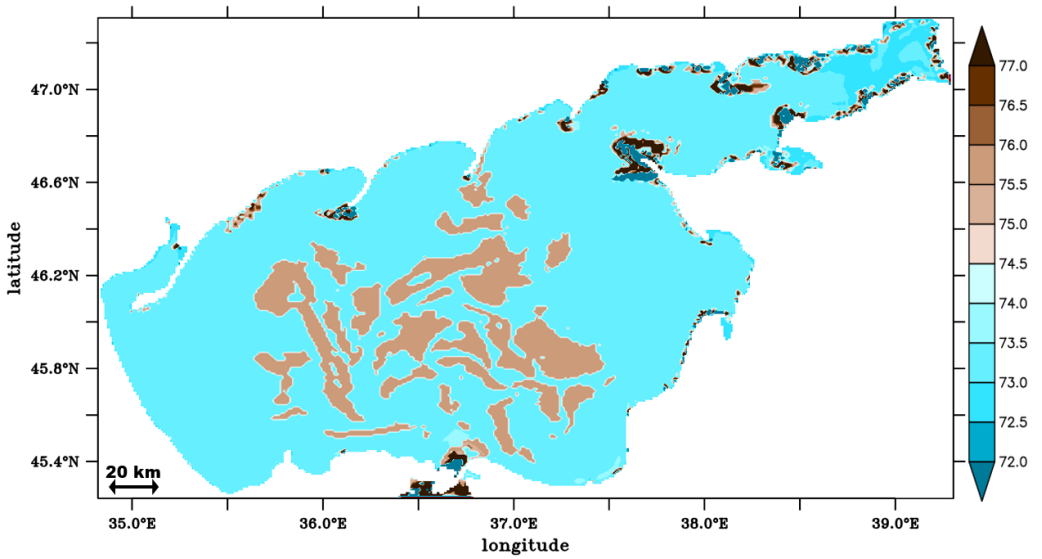

Figure 9: Average mud fraction (%) in the sediment at July 1st, 2021, with an initial mean over sediment thickness mud fraction set at 77.6%.

ing from an initial homogeneous value of 77.6% to a heterogeneous range of 72-77% after one month. Dark brown areas with the highest mud fraction correspond to deposition areas depicted in Fig. 7 and Fig. 8, exhibiting the highest sediment thickness and the lowest sediment dry density (indicating fresh sediment). Light brown areas in the central part of the figure indicate regions where the sediment has remained thicker and less dense, indicating a higher concentration of mud particles. These areas are primarily characterized by a combination of moderate consolidation and deposition processes.

In contrast, light blue colors represent areas with a slightly lower mud fraction, thinner sediment layers (as shown in Fig. 7), and higher dry density (as shown in Fig. 8). These regions are dominated by moderate consolidation and erosion processes. The variations in mud fraction reveal the spatial heterogeneity of sediment properties, highlighting the combined influence of consolidation, deposition, and erosion on the distribution of mud particles in the study area.

5.4. Pathways and locations of the SPM settlement

The interaction between global circulation and particle settlement plays a crucial role in the advection of floating particles. While the global circulation

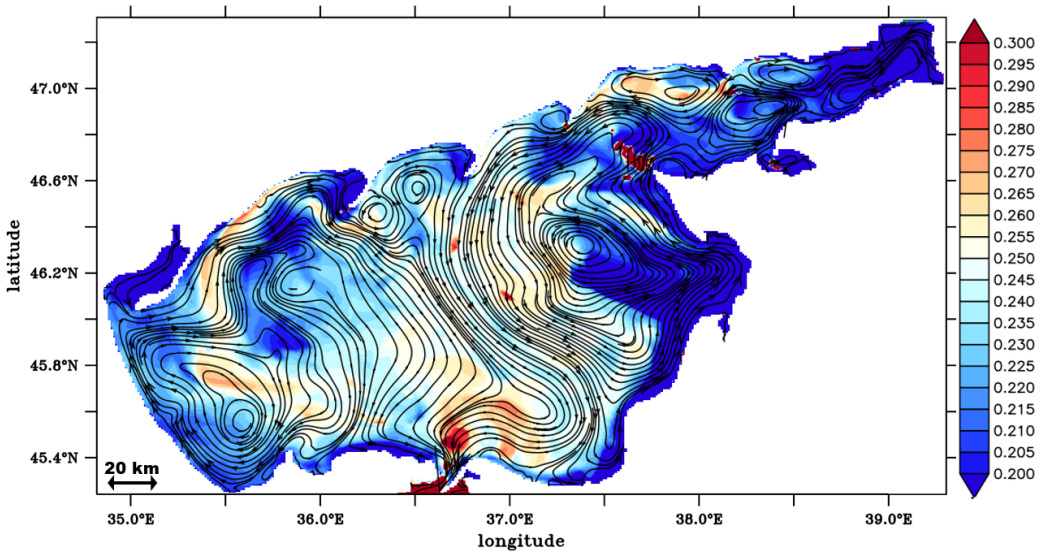

Figure 10: Maximal vertical SPM concentration (in g/l) represented by colors at July 1st, 2021, and barotropic flows, averaged over the month of June 2021.

is responsible for horizontal transport, particle settlement, determined by its weight, contributes to vertical transport. However, the combined influence of these two processes is not yet fully understood. By examining the average current distribution and identifying areas of high SPM concentration near the seabed, we can find potential regions of particle resettlement.

In Fig. 10, the distribution of SPM in the water column is depicted, representing the maximum concentration achieved after one month of simulation under various forcing conditions. Additionally, the mean pathways of SPM advection during the past month are illustrated. The simulation reveals the presence of two large gyres in the central part of the Azov Sea: an eastern gyre (smaller and rotating anticlockwise) and a western gyre (larger and rotating clockwise). These gyres serve as conduits for suspended matter originating from the Don River and eroded from the shores. The eastern gyre feeds into the western gyre in the southeastern region of the Azov Sea, contributing to the transport of suspended solids. The highest concentrations of SPM, reaching approximately 0.25-0.3 g/l, are predominantly observed in the central part of the Azov Sea, as well as the western side of the Sea.

Fig. 11 illustrates the depth at which the maximum concentration of suspended particles occurs after one month of simulation. It should be noted

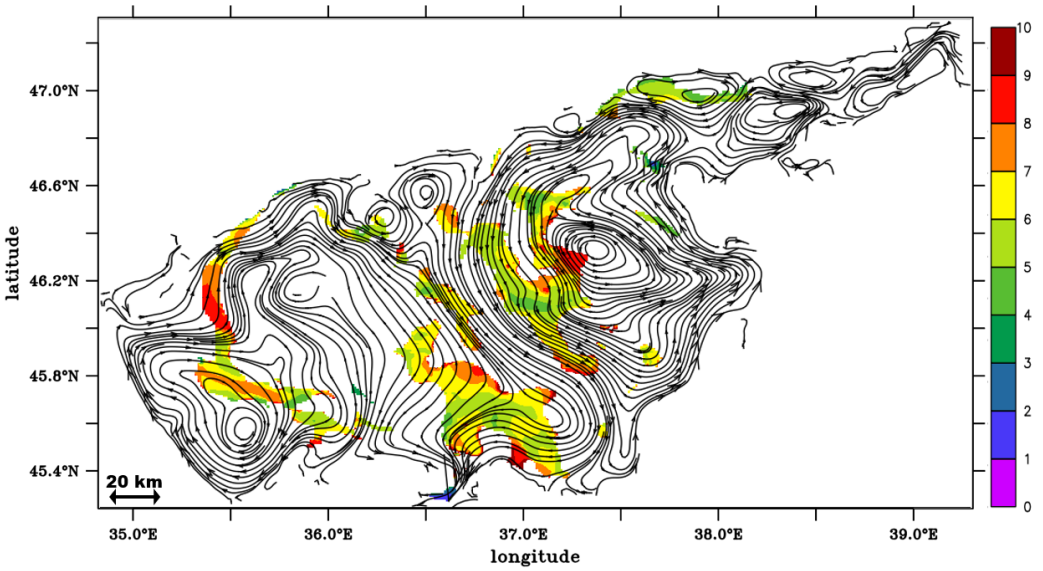

Figure 11: Colors represent the depth (in meters) of the maximal vertical SPM concentration of 0.25 g/l at July 1st, 2021, while flows denote barotropic flows averaged over the month of June 2021.

that this concentration primarily consists of clay particles, comprising 99% of the total (not shown in the figure). The transport of particles is influenced by two processes: current advection and particle settlement. Consequently, the greatest depths of maximal concentration correspond to the ultimate deposition locations, where particles have settled onto the seabed. Regions depicted in red indicate the highest concentrations of suspended particles near the bottom. These areas are primarily located in the western side of the eastern gyre, as well as the southeastern and western sides of the western gyre.

6. Discussion and Conclusion

The latest results on complex transport patterns of fine particles, influenced by both currents and settlement processes, highlight the need for comprehensive modeling approaches to accurately represent these dynamics.

The study began by comparing suspended sediment concentrations from the 3D model with satellite data. The model showed good agreement with the satellite observations, indicating its reliability and suitability for our research.

During the one-month period encompassing multiple extreme events, several conclusions were drawn.

We analyzed sediment stocks and fluxes in the Taganrog Bay, considering the combined influences of wind and river. Our study revealed that clay particles remained suspended throughout the simulation due to their low settlement velocity, while particles from other fractions (predominantly the medium fraction) were only suspended during strong wind events and quickly settled afterward. Wind stress above 0.05 Pa caused particulate matter erosion, resulting in its presence in the water column.

We examined sediment characteristics to identify erosion-prone and deposition-prone areas. After extreme events within the one-month period, the coastal regions of the Taganrog Bay experienced significant erosion, characterized by thin sediment layers and high dry density. Deposition areas, with thicker sediment layers and lower dry density, were often located near the erosion zones. The predominance of heavier particles in the medium silt fraction contributed to their quick settlement, influencing the proximity of deposition areas to erosion sites. In the central part of the sea, sediment layers were moderately thicker, containing a higher mud fraction. This region served as a zone for the accumulation of fine sediments, including fine silt and clay, which remained suspended for longer durations and were transported over greater distances by ocean currents.

The identification of two major gyres, namely an eastern and a western gyre, aligns with the well-documented circulation patterns established within the Azov Sea. The eastern gyre's contribution to sediment load in the western gyre emphasizes the interconnectedness of these regions and the potential for long-distance transport of suspended solids. These gyres play a crucial role in redistributing particles and influencing the overall sediment distribution in the sea.

The areas with the highest concentrations of fine particles, primarily composed of clay, demonstrate the importance of these regions as settling zones. Understanding the depth of maximal concentration and identifying the final deposition sites provides valuable information for assessing potential impacts on benthic ecosystems and sediment accumulation rates.

The observed variations in sediment thickness, dry density, and mud fraction across the study area further emphasize the spatial heterogeneity of sediment characteristics. The higher erosion rates in certain areas lead to thinner sediment layers and higher dry densities, while deposition areas exhibit thicker sediment layers and lower dry densities.

In conclusion, it is noteworthy that our findings align with prior studies, highlighting that robust winds, particularly during storms, play a significant role in driving substantial sediment redistribution in shallow coastal waters. The mechanism behind this phenomenon encompasses a wind-induced surge in wave power, sediment resuspension, and advection (e.g., Yang et al., 2023). Moreover, our study unveils distinct responses of sediment fractions to the impact of storms or wind. We posit that these findings have significant implications for coastal erosion and accretion processes, contributing valuable information to comprehend the overall sediment budget in the Azov Sea.

In future research, a deeper investigation should explore how intricate hydrodynamic conditions in shallow bays influence the transport of sediment particles of varying sizes, with a specific focus on strong wind characteristics. This should include a comparative analysis of the transport and response features of multi-component sediments during various strong wind events.

Overall, we believe that this study offers a new knowledge into the pathways and locations of SPM settlement in the Azov Sea. The intricate interplay between currents, settlement processes, erosion events, and river influx emphasizes the necessity for a comprehensive understanding of these dynamics to accurately assess their ecological and environmental implications. The findings contribute to the knowledge base essential for effective management and conservation strategies in this semi-enclosed sea.

Acknowledgements

Centre de Calcul Intensif d'Aix-Marseille is acknowledged for granting access to its high performance computing resources.

References

[1] Alekseenko E., Roux B., 2020. Risk of wind-driven resuspension and transport of contaminated sedimentsin a narrow marine channel confluencing a wide lagoon. Estuarine Coastal and Shelf Science, 237. https://doi.org/10.1016/j.ecss.2020.106649

[2] Alekseenko E. and Roux B., 2019. Wind effect on bottom shear stress, erosion and redeposition on Zostera noltei restoration in a coastal lagoon; part 2. Estuarine, Coastal and Shelf Science, 216, 14-26. https://doi.org/10.1016/j.ecss.2018.05.022

[3] Arkema, K. K., Guannel, G., Verutes, G., Wood, S. A., Guerry, A., Ruckelshaus, M., ... & Tallis, H., 2013. Coastal habitats shield people and property from sea-level rise and storms. Nature Climate Change, 3(10), 913-918

[4] Arkhipov B. V., Koterov V. N., Solbakov V. V., Yurezanskaya Yu. S., 2010. Simulation of suspended substance transport on the continental shelf: Computation of soil dumping in the Sea of Azov, Zh. Vychisl. Mat. Mat. Fiz., 50:4, 746–756; Comput. Math. Math. Phys., 50:4 (2010), 711–720

[5] Barbier, E. B., Hacker, S. D., Kennedy, C., Koch, E. W., Stier, A. C., & Silliman, B. R., 2011. The value of estuarine and coastal ecosystem services. Ecological Monographs, 81(2), 169-193

[6] Bartholomeeusen G., Sills G.C., Znidarcic D., Van Kesteren W., Merckelbach L.M., Pyke R., Carrier W.D., Lin H., Penumadu D., Winterwerp H., et al., 2002. Sidere: Numerical prediction of large-strain consolidation. Géotechnique 2002, 52, 639–648

[7] Berdnikov, S.V., Dashkevich, L.V., Kulygin, V.V., Sheverdyaev, I.V., Tretyakova, I.A., & Yaitskaya, N.A., 2018. Ex-Mare - Forecasting System Of Natural Hazards In The Azov Sea Region. Geography, Environment, Sustainability, 11(2), 29-45. DOI: 10.24057/2071-9388-2018-11-2-29-45

[8] Berenbrock, C., Tranmer, A.W., 2008. Simulation of Flow, Sediment Transport, and Sediment Mobility of the Lower Coeur d'Alene River, Idaho; Scientific Investigations Report; U.S. Environmental Protection Agency: Washington, DC, USA, 2008; pp. 2008–5093

[9] Cayocca F., Verney R., Petton S., Caillard M., Dussauze M., Dumas F., Le Roux J.-F., Pineau L., Le Hir P., 2014. Development and Validation of a Sediment Dynamics Model within a Coastal Operational Oceanographic System. Mercat. Ocean.-Q. Newsl. 2014, 49, 76–86

[10] Chichaeva M.A., Lychagin M.Yu., Syroeshkin A.V., Chernitsova O.V., 2020. Heavy Metals In Marine Aerosols Of The Azov Sea. GEOGRAPHY, ENVIRONMENT, SUSTAINABILITY. 2020;13(2):127-134. https://doi.org/10.24057/2071-9388-2020-11

[11] Colosimo, I., van Maren, D. S., de Vet, P. L. M., Winterwerp, J. C., van Prooijen, B. C., 2023. Winds of opportunity: the effects of wind on intertidal flat accretion. Geomorphology, 439, 108840

[12] Dankers P.J.T., Winterwerp J.C., 2007. Hindered settling of mud flocs: Theory and validation. Cont. Shelf. Res. 2007, 27, 1893–1907

[13] Diaz M., Grasso F., Le Hir P., Sottolichio A., Caillaud M., Thouvenin B., 2020. Modeling mud and sand transfers between a macrotidal estuary and the continental shelf: Influence of the sediment-transport parameterization. J. Geophys. Res. Oceans 2020,125, e2019JC015643

[14] Duarte, C. M., Losada, I. J., Hendriks, I. E., Mazarrasa, I., & Marbà, N., 2013. The role of coastal plant communities for climate change mitigation and adaptation. Nature Climate Change, 3(11), 961-968

[15] Grasso F., Le Hir P., Bassoullet P., 2015. Numerical modelling of mixed-sediment consolidation. Ocean. Dyn. 2015, 65, 607–616

[16] IPCC, 2022. Climate Change 2022: Impacts, Adaptation, and Vulnerability. Contribution of Working Group II to the Sixth Assessment Report of the Intergovernmental Panel on Climate Change [H.-O. Pörtner, D.C. Roberts, M. Tignor, E.S. Poloczanska, K. Mintenbeck, A. Alegría, M. Craig, S. Langsdorf, S. Löschke, V. Möller, A. Okem, B. Rama (eds.)]. Cambridge University Press. Cambridge University Press, Cambridge, UK and New York, NY, USA, 3056 pp., doi:10.1017/9781009325844

[17] Ivlieva O.V., and Berdnikov S.V., 2005. Recent destruction rates of the Azov beaches in Russia. Geomorphology RAS. (4), pp. 74-83. DOI:10.15356/0435-4281-2005-4-74-83

[18] Klenkin, A.A. & S.A. Agapov. 2011. Dynamics of the distribution of petroleum hydrocarbons in the water and bottom sediments of the Sea of Azov and of the Black Sea after the accident in the Kerch Strait. Vodnye Resursy 38(2): 214-222

[19] Lazure P., Dumas F., 2008. An external-internal mode coupling for a 3D hydrodynamical model for applications at regional scale (MARS). Adv. Wat. Res. 2008, 31, 233–250

[20] Lazure P., Garnier V., Dumas F., Herry C., Chifflet M., 2009. Development of a hydrodynamic model of the Bay of Biscay. Validation of hydrology. Cont. Shelf Res. 2009, 29, 985–997

[21] Le Hir P., Cayocca F., Waeles B., 2011. Dynamics of sand and mud mixtures: A multiprocess-based modelling strategy. Cont. Shelf Res. 2011, 31, S135–S149

[22] Martinez, M.L., Intralawan, A., Vazquez, G., Perez-Maqueo, O., Sutton, P., & Landgrave, R., 2007. The coasts of our world: Ecological, economic and social importance. Ecological Economics, 63(2-3), 254-272. https://doi.org/10.1016/j.ecolecon.2006.10.022

[23] Matishov, G.G. and Matishov, D.G., 2013. Current Natural and Social Risks in the Azov-Black Sea Region. Herald of the Russian Academy of Sciences, [e-journal] 83(6), pp. 490-498. doi:10.1134/S1019331613090062

[24] Mengual B., Le Hir P., Cayocca F., Garlan T., 2017. Modelling fine sediment dynamics: Towards a common erosion law for fine sand, mud and mixtures. Water 2017, 9, 564

[25] Merckelbach L., Kranenburg C., 2004. Equations for effective stress and permeability of soft mud-sand mixtures. Géotechnique 2004, 54, 235–243

[26] Partheniades E., 1965. Erosion and deposition of cohesive soils. J. Hydraul. 1965, 91, 105–139

[27] Sorokina, V.V., Berdnikov, S.V., 2008. Mathematical modeling of the terrigenous sedimentation in the Sea of Azov. Oceanology 48, 418–427 (2008). https://doi.org/10.1134/S0001437008030144

[28] Soulsby R.L., 1997. Dynamics of Marine Sands: A Manual for Practical Applications; Thomas Telford: London, UK, 1997; ISBN 0-7277-2584-X

[29] USDA. US Department of Agriculture: Soil Bulk Density/Moisture/Aeration. 2014. Available online: https://www.nrcs.usda.gov

[30] Waeles B., Le Hir P., Lesueur P., Delsinne N., 2007. Modelling sand/mud transport and morphodynamics in the Seine river mouth (France): an attempt using a process-based approach. Hydrobiologia 2007, 588, 69–82

[31] Yaitskaya, N., 2022. The Wave Climate of the Sea of Azov. Water, 14(4), 555. https://doi.org/10.3390/w14040555

[32] Yang, SL, X. Luo, S. Temmerman, M. Kirwan, T. Bouma, K. Xu, S. Zhang, J. Fan, B. Shi, H. Yang, YP Wang, X. Shi, S. Gao, 2020. Role of delta-front erosion in sustaining salt marshes under sea-level rise and fluvial sediment decline. Limnology and Oceanography. 65 (9), 1990-2009

[33] Yang, S., T.J. Bouma, K. Xu, B. Shi, H. Yang, W. Zhan, X. Luo, P. Li, Y. Huang, M. Tian, L. Gu, Z. Dai, 2023. Storms dominate the erosion of the Yangtze Delta and southward sediment transport. Science Bulletin, 68(6), 553-556.